

# Boundary-Controlled Liouvillian Relaxation with Exact Steady States Fixed by Dissipative Disorder

Y. Z. Miao,<sup>1</sup> W. Z. Ma,<sup>1</sup> Y. Wang,<sup>1</sup> X. L. Zhao,<sup>1,\*</sup> and X. X. Yi<sup>2,†</sup>

<sup>1</sup>*School of Science, Qingdao University of Technology, Qingdao, Shandong, China*

<sup>2</sup>*Center for Quantum Sciences and School of Physics, Northeast Normal University, Changchun, Jilin, China*

In open quantum lattice systems, changing the boundary condition would appear to alter both the steady state and the nonzero Liouvillian spectrum. Here we show that boundary conditions can be used to control relaxation without changing the reduced steady state. In a disordered dissipative quantum link chain, the steady state is determined by an accumulated field defined by link-resolved dissipative disorder, and a gauge-generated transformation built from this field gives exact symmetry-resolved steady states with nonuniform, accumulated-field-dependent reduced matter occupations. We then construct a reciprocal cyclic boundary condition that preserves these matter occupations while changing the nonzero Liouvillian spectrum. Consequently, open and cyclic chains relax to the same reduced matter steady-occupation profile with different Liouvillian gaps with the cyclic closure accelerating relaxation. In the strong-dissipation limit, this relaxation difference can be reduced to a spectral comparison of effective exclusion processes with open and cyclic boundaries.

*Introduction.*— Boundary sensitivity is well known in discussions of non-Hermitian skin effects, where changing the boundary condition can reshape the spectrum and eigenmode profiles [1–12]. In open quantum lattice systems, the same boundary sensitivity directly affects Lindbladian relaxation: the boundary condition can modify both the steady state and the nonzero Liouvillian modes that govern the relaxation toward it [13–15]. When these two changes occur together, the observed relaxation cannot be assigned uniquely to a changed steady state or to a changed nonzero spectrum.

Removing this ambiguity requires a steady observable that remains fixed when the boundary condition is changed. Globally reciprocal non-Hermitian systems show how such boundary-insensitive profiles can arise when local nonreciprocal biases with vanishing global bias produce realization-dependent profiles controlled by an accumulated field [16–18]. Extending this accumulated-field control to interacting open quantum systems is nontrivial. Related many-body skin phenomena have been studied in systems with dynamical gauge couplings [19, 20], exactly solvable interacting nonreciprocal dynamics [21], and boundary-sensitive Liouvillian chains [14, 22]. However, for disordered interacting dissipative chains, exact steady states and boundary-resolved nonzero Liouvillian spectra are generally unavailable. It therefore remains unclear whether a disordered accumulated field can fix the occupation of matter at steady state while the boundary condition changes the nonzero Liouvillian spectrum.

Quantum link chains provide the candidate for addressing this question. Link-local dissipation defines local dissipative asymmetries, while constrained matter-link exchange relates the corresponding link weights to matter-site weights. This structure follows from gauge constraints, which couple matter and link degrees of freedom and restrict the allowed dynamics [23–25], and is

naturally formulated within finite-dimensional quantum link models [26]. Relevant gauge dynamics has been implemented or proposed in ultracold atoms [27–30], trapped ions [31, 32], Rydberg arrays [33], and superconducting circuits [34, 35], with parallel progress in gauge protection [36–39], controlled dissipation [40, 41], and dissipative gauge steady states [42, 43]. In the uniformly biased case, dissipative quantum link models admit exact many-body skin steady states [44], motivating the dissipative quantum link chain with globally reciprocal link-dissipation disorder studied here.

Here we focus on a chain with locally asymmetric but globally reciprocal link dissipation. We show that the disordered dissipative asymmetries define an accumulated field, from which a gauge-generated transformation gives exact symmetry-resolved steady states under open boundary conditions (OBC) and accumulated-field ordered reduced matter steady occupations. We then construct a reciprocal cyclic boundary condition (CBC), which preserves the OBC reduced matter steady occupation but changes the nonzero Liouvillian spectrum, thereby modifying the Liouvillian gap and the late-time matter-occupation relaxation rate. This separates the accumulated-field control of the steady occupation from the boundary control of relaxation, and the separation admits a concise spectral interpretation in terms of effective open and cyclic exclusion processes in the strong-dissipation limit.

*Model and symmetries.*— We first consider a one-dimensional  $U(1)$  quantum link chain with  $L$  matter sites and OBC [26, 45, 46]. In the fermionic form, the coherent Hamiltonian is  $H_f = J \sum_{n=1}^{L-1} (\psi_n^\dagger U_{n,n+1} \psi_{n+1} + \text{H.c.})$ , where  $\psi_n$  acts on matter site  $n$ , and  $U_{n,n+1}$  is conjugate to the electric field  $E_{n,n+1}$ , satisfying  $[E_{n,n+1}, U_{n,n+1}] = U_{n,n+1}$  and  $[E_{n,n+1}, U_{n,n+1}^\dagger] = -U_{n,n+1}^\dagger$ . With the links oriented from left to right, the lattice divergence of the electric field at a bulk site is  $E_{n,n+1} - E_{n-1,n}$ .

The fermionic Gauss-law generators are therefore  $\mathcal{G}_n^f = \psi_n^\dagger \psi_n - (E_{n,n+1} - E_{n-1,n})$  for  $1 < n < L$ , with boundary forms  $\mathcal{G}_1^f = \psi_1^\dagger \psi_1 - E_{1,2}$  and  $\mathcal{G}_L^f = \psi_L^\dagger \psi_L + E_{L-1,L}$ . For fixed static background charges  $g_n$ , the Gauss-law sector is the simultaneous eigenspace of the local generators satisfying  $\mathcal{G}_n^f |\Phi\rangle = -g_n |\Phi\rangle$  for all sites  $n$ .

After representing the quantum links by spin operators and applying the Jordan–Wigner transformation to the matter fields [44–46], the Hamiltonian  $H_f$  becomes

$$H = J \sum_{n=1}^{L-1} (\tau_n^+ s_{n,n+1}^+ \tau_{n+1}^- + \text{H.c.}). \quad (1)$$

In this correlated exchange form,  $\tau_n^\pm$  act on matter site  $n$ , while  $s_{n,n+1}^\pm$  act on the intervening link  $(n, n+1)$ , with  $s_{n,n+1}^z$  representing the electric field and  $[s_{n,n+1}^z, s_{m,m+1}^\pm] = \pm \delta_{nm} s_{m,m+1}^\pm$ . We take the minimal link spins  $s = 1/2$  throughout. The matter occupation and total matter number are  $\hat{n}_n = \tau_n^+ \tau_n^- = \tau_n^z + 1/2$  and  $\hat{N} = \sum_{n=1}^L \hat{n}_n$ , so that  $\tau_n^z = 1/2$  ( $-1/2$ ) denotes an occupied (empty) site. After absorbing the uniform matter offset into the static background charges, the spin Gauss generators are

$$G_n = \tau_n^z - (s_{n,n+1}^z - s_{n-1,n}^z), \quad 1 < n < L. \quad (2)$$

For the two open boundaries, we have  $G_1 = \tau_1^z - s_{1,2}^z$  and  $G_L = \tau_L^z + s_{L-1,L}^z$ . The spin Gauss generators satisfy  $[G_n, H] = 0$  and  $\sum_{n=1}^L G_n = \sum_{n=1}^L \tau_n^z = \hat{N} - L/2$ .

The coherent dynamics described by Eq. (1) is a gauge-invariant correlated exchange between matter and link degrees of freedom, while the dissipation is taken to act directly on the links, as illustrated in Fig. 1. The open-system dynamics is governed by

$$\begin{aligned} \frac{d\rho}{dt} = \mathcal{L}[\rho] = & -i[H, \rho] \\ & + \sum_{n=1}^{L-1} \sum_{\mu=u,d} \left( 2L_n^{(\mu)} \rho L_n^{(\mu)\dagger} - \{L_n^{(\mu)\dagger} L_n^{(\mu)}, \rho\} \right). \end{aligned} \quad (3)$$

We decompose  $\mathcal{L} = \mathcal{L}_H + \mathcal{L}_D$ , with  $\mathcal{L}_H[\rho] \equiv -i[H, \rho]$  and  $\mathcal{L}_D$  denoting the dissipative part in Eq. (3), in which  $L_n^{(u)} = \sqrt{\gamma_{u,n}} s_{n,n+1}^+$  and  $L_n^{(d)} = \sqrt{\gamma_{d,n}} s_{n,n+1}^-$ . The local dissipative asymmetry on link  $n$  is denoted by  $h_n = \ln(\gamma_{u,n}/\gamma_{d,n})$ . Equivalently,  $\gamma_{u,n} = \gamma e^{h_n/2}$  and  $\gamma_{d,n} = \gamma e^{-h_n/2}$ , with  $\gamma > 0$  setting the overall dissipation scale. We consider the globally reciprocal case

$$\sum_{n=1}^{L-1} h_n = 0, \quad (4)$$

so that the total dissipative asymmetry vanishes while finite local disordered dissipative asymmetries on the links are retained.

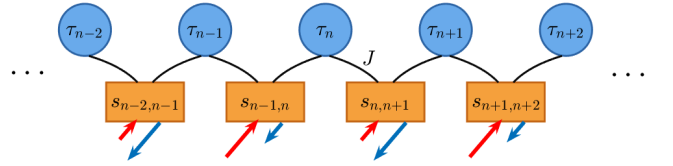


FIG. 1. Dissipative  $U(1)$  quantum link chain. Blue circles denote matter spins  $\tau_n$ , orange rectangles denote link spins  $s_{n,n+1}$ , black curves denote the coherent coupling  $J$ , and red/blue arrows denote link pumping and loss.

The jump operators break the strong gauge symmetry generated by  $G_n$ , but preserve a weak Liouvillian symmetry. Defining the weak-gauge superoperator  $\mathcal{W}_n[\rho] \equiv G_n \rho - \rho G_n$ , one has  $[\mathcal{W}_n, \mathcal{L}] = 0$ . The matter number remains a strong symmetry because  $[\hat{N}, H] = 0$  and  $[\hat{N}, L_n^{(\mu)}] = 0$ . The Liouvillian therefore decomposes in operator space into blocks labeled by the eigenvalues of  $\mathcal{W}_n$  and by the conserved matter number. The steady states and spectra considered below are evaluated in the zero weak-gauge block  $\mathcal{W}_n[\rho] = 0$  at fixed matter number  $N$ .

*Accumulated-field steady state.*— We construct the exact OBC steady state by extending the link-space transformation of the dissipator to a gauge-generated transformation on the matter-link chain. Since  $\mathcal{L}_D$  acts independently on different links, its steady state in the link sector is diagonal and factorizes as

$$\rho_s = \bigotimes_{n=1}^{L-1} \rho_{n,n+1}, \quad \rho_{n,n+1} = \frac{e^{h_n} |\uparrow\rangle \langle \uparrow| + |\downarrow\rangle \langle \downarrow|}{1 + e^{h_n}}, \quad (5)$$

where  $|\uparrow\rangle$  and  $|\downarrow\rangle$  are the  $\pm 1/2$  eigenstates of  $s_{n,n+1}^z$ . The diagonal weights in Eq. (5) determine the diagonal link-space transformation  $T_s = \bigotimes_{n=1}^{L-1} T_{n,n+1}$ , with  $T_{n,n+1} \propto e^{-h_n s_{n,n+1}^z}$ , which maps  $\rho_s$  to the identity,  $T_s \rho_s \propto I_s$ . With the left-multiplication superoperator  $\mathcal{T}_s[\rho] = T_s \rho$ , applying this link-space transformation to each local link dissipator gives  $\mathcal{T}_s \mathcal{L}_D \mathcal{T}_s^{-1} = \mathcal{L}_D^\dagger$ .

The link factors  $e^{-h_n s_{n,n+1}^z}$  alone would rescale the correlated exchange terms in Eq. (1). To extend the link-space transformation to a gauge-generated transformation that leaves these terms invariant, the matter-site weights must satisfy nearest-neighbor differences equal to the local dissipative asymmetries  $h_n$ . We therefore introduce the accumulated field

$$X_1 = 0, \quad X_n = \sum_{m=1}^{n-1} h_m, \quad n \geq 2, \quad (6)$$

thus  $X_{n+1} - X_n = h_n$ . We use the gauge-generated transformation  $T = \exp[-\sum_{n=1}^L (\ln \alpha + X_n) G_n]$ , where  $\alpha > 0$  is an arbitrary constant. Using Eq. (2), the exponent decomposes as  $\sum_{n=1}^L (\ln \alpha + X_n) G_n = \sum_{n=1}^L (\ln \alpha + X_n) \tau_n^z + \sum_{n=1}^{L-1} (X_{n+1} - X_n) s_{n,n+1}^z$ . Since  $X_{n+1} - X_n = h_n$ , the

link part of  $T$  differs from  $T_s$  only by an overall scalar factor. Equation (4) gives  $X_L = X_1 = 0$ , while the intermediate partial sums in Eq. (6) depend on the disorder realization and define the accumulated-field profile.

Since  $\mathcal{L}_D$  acts only on the links and the link part of  $T$  matches  $T_s$  up to an overall scalar factor, the left-multiplication superoperator  $\mathcal{T}[\rho] = T\rho$  gives  $\mathcal{T}\mathcal{L}_D\mathcal{T}^{-1} = \mathcal{L}_D^\dagger$ . Since  $[G_n, H] = 0$  for all  $n$ , the transformation leaves the Hamiltonian (1) invariant,  $THT^{-1} = H$ . Namely, the factors generated on  $\tau_n^+$ ,  $s_{n,n+1}^+$ , and  $\tau_{n+1}^-$  cancel inside each correlated exchange term. Hence  $\mathcal{T}\mathcal{L}\mathcal{T}^{-1} = \mathcal{L}_H + \mathcal{L}_D^\dagger$ . Because  $\mathcal{L}_H[I] = 0$  and  $\mathcal{L}_D^\dagger[I] = 0$ , the identity is a steady operator of the transformed Liouvillian. Transforming back gives the exact OBC steady state

$$\rho_{\text{ss}} = \frac{\mathcal{T}^{-1}[I]}{\text{Tr}\{\mathcal{T}^{-1}[I]\}} = Z^{-1} \exp \left[ \sum_{n=1}^L (\ln \alpha + X_n) G_n \right]. \quad (7)$$

Since  $\sum_{n=1}^L G_n = \hat{N} - L/2$ , the term  $\ln \alpha \sum_n G_n = \ln \alpha (\hat{N} - L/2)$  depends only on the conserved matter number. Thus  $\ln \alpha$  can be viewed as the chemical potential of a Gibbs ensemble. After projection to a fixed eigenvalue  $N$  of  $\hat{N}$ ,  $\ln \alpha$  is a constant and is removed by normalization. The symmetry-resolved OBC steady state in the fixed- $N$  sector is therefore

$$\rho_{\text{ss},N} = Z_N^{-1} P_N \exp \left[ \sum_{n=1}^L X_n G_n \right] P_N, \quad (8)$$

where  $P_N$  projects onto the eigenspace of  $\hat{N}$  with eigenvalue  $N$ , and  $Z_N = \text{Tr}\{P_N \exp[\sum_{n=1}^L X_n G_n] P_N\}$ .

The fixed- $N$  reduced matter distribution is obtained by tracing out the link spins in Eq. (8). In the exponent  $\sum_{\ell=1}^L X_\ell G_\ell$ , the link contribution is  $\sum_{q=1}^{L-1} (X_{q+1} - X_q) s_{q,q+1}^z$  and gives a matter-configuration-independent factor after tracing out the link degrees of freedom. The matter contribution is  $\sum_{\ell=1}^L X_\ell \tau_\ell^z$ . For a matter occupation configuration  $\mathbf{a} = (a_1, \dots, a_L)$ , where  $a_\ell = 0, 1$  is the occupation of site  $\ell$ , one has  $\tau_\ell^z = a_\ell - 1/2$ . The factors independent of  $\mathbf{a}$  are absorbed into the normalization, and the fixed- $N$  reduced matter distribution is

$$p_N(\mathbf{a}) = \delta_{(\sum_{\ell=1}^L a_\ell, N)} \frac{\exp\left(\sum_{\ell=1}^L X_\ell a_\ell\right)}{Z_N^m}, \quad (9)$$

with  $Z_N^m = \sum_{\mathbf{a}} \delta_{(\sum_{\ell=1}^L a_\ell, N)} \exp\left(\sum_{\ell=1}^L X_\ell a_\ell\right)$ . The site-resolved reduced matter steady occupation is  $N_n^{\text{ss}} \equiv \text{Tr}[\rho_{\text{ss},N} \hat{n}_n] = \sum_{\mathbf{a}} p_N(\mathbf{a}) a_n$ .

To show how the accumulated field orders the site occupations, compare two distinct matter sites  $i \neq j$  for  $0 < N < L$ . From Eq. (9),  $N_i^{\text{ss}} - N_j^{\text{ss}} = \sum_{\mathbf{a}} p_N(\mathbf{a}) (a_i - a_j)$ . Only configurations with  $(a_i, a_j) = (1, 0)$  or  $(0, 1)$  contribute to  $N_i^{\text{ss}} - N_j^{\text{ss}}$ . For each admissible remaining configuration  $\mathbf{b} = \{b_\ell\}_{\ell \neq i, j}$  satisfying  $\sum_{\ell \neq i, j} b_\ell = N - 1$ , the

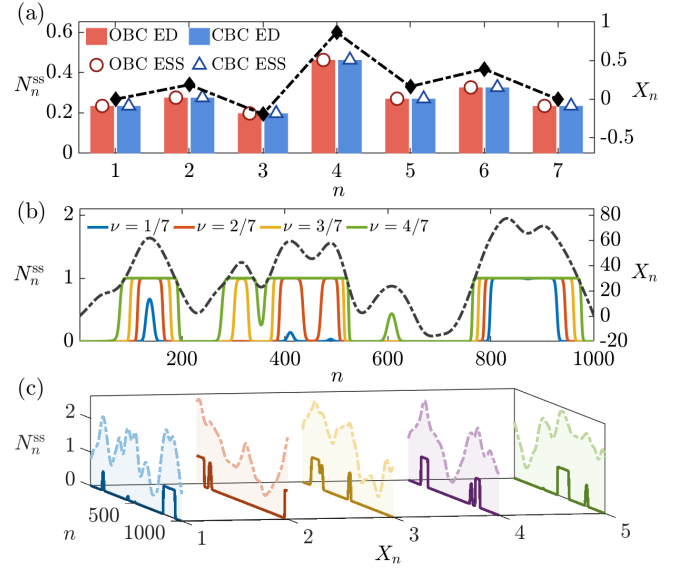


FIG. 2. Accumulated-field control of  $N_n^{\text{ss}}$ . In all panels,  $N_n^{\text{ss}}$  is plotted against the left axis and the accumulated field  $X_n$  against the right axis. (a)  $L = 7$ ,  $N = 2$ : bars show OBC and CBC values of  $N_n^{\text{ss}}$  from exact diagonalization, markers show the corresponding values from exact symmetry-resolved steady states, and the dash-dotted curve shows  $X_n$ . (b) OBC  $N_n^{\text{ss}}$  from the exact reduced matter distribution for a separate  $L = 1001$  realization at  $\nu \equiv N/L = 1/7, 2/7, 3/7, 4/7$ ; the dash-dotted curve shows  $X_n$  for the same realization. (c) OBC  $N_n^{\text{ss}}$  from the exact reduced matter distribution for five realizations with  $L = 1001$ ,  $N = 143$ ; dash-dotted curves show the corresponding  $X_n$ . Parameters are  $J = 1$  and  $\gamma = 2$ . For each realization, the interior asymmetries  $h_n$  are constructed from globally reciprocal Gaussian disorder realizations with exact sample mean zero and sample variance  $\sigma_h^2 = 0.4$ .

two contributing configurations  $(a_i, a_j) = (1, 0)$  and  $(0, 1)$  have weights proportional to  $e^{X_i} \exp(\sum_{\ell \neq i, j} X_\ell b_\ell)$  and  $e^{X_j} \exp(\sum_{\ell \neq i, j} X_\ell b_\ell)$ , respectively. Subtracting their contributions and summing over all admissible  $\mathbf{b}$  gives

$$N_i^{\text{ss}} - N_j^{\text{ss}} = \frac{(e^{X_i} - e^{X_j}) W_{N-1}^{(i,j)}}{Z_N^m}, \quad (10)$$

with  $W_{N-1}^{(i,j)} = \sum_{\mathbf{b}} \delta_{(\sum_{\ell \neq i, j} b_\ell, N-1)} \exp(\sum_{\ell \neq i, j} X_\ell b_\ell) > 0$ . Thus

$$X_i > X_j \iff N_i^{\text{ss}} > N_j^{\text{ss}}. \quad (11)$$

Equations (9) and (11) give the accumulated-field control of the matter steady-occupation profile. In Fig. 2(a), the OBC  $N_n^{\text{ss}}$  from Eq. (9) agrees with exact diagonalization in the zero weak-gauge block at fixed matter number, and the profile is ordered by  $X_n$ . For another realization of  $X_n$ , Fig. 2(b) shows that changing the filling factor redistributes the occupation over the same accumulated-field profile, with the site occupations following Eq. (11). Across different globally reciprocal disorder realizations,

Fig. 2(c) shows that different accumulated-field  $X_n$  produce different OBC matter steady-occupation profiles, each ordered according to Eq. (11). Thus the many-body erratic steady occupation is controlled by the realization-dependent accumulated field.

*Reciprocal boundary condition and Liouvillian branches.*— In boundary-sensitive open systems, changing the boundary generally changes both the fixed- $N$  reduced matter steady-state distribution and the nonzero Liouvillian spectrum [15, 44]. Equation (9) shows that the two boundary responses can be disentangled at the steady-state level: this distribution is preserved if the matter-site values  $\{X_n\}$  are kept unchanged. We therefore close the chain by imposing cyclic consistency on the accumulated field.

We implement this closure by keeping the  $L-1$  interior links fixed and adding a single link between sites  $L$  and 1. Let  $J_b$  denote the coherent correlated-exchange coupling strength on the closing link, and let  $h_L$  denote its local dissipative asymmetry. Keeping the interior values of  $X_n$  fixed, a single-valued accumulated field on the cycle means  $X_{L+1} = X_1$ , equivalently  $\sum_{n=1}^L h_n = 0$ . Since the interior realization already satisfies Eq. (4), the added link must have  $h_L = 0$ ,  $\gamma_{u,L} = \gamma_{d,L} \equiv g_0$ , where  $g_0 > 0$ . Throughout this work we set  $g_0 = \gamma$  and  $J_b = J$ . Thus, within this single-link closure scenario, cyclic consistency of the accumulated field determines the reciprocal dissipative closing link, while the coherent exchange is closed with the same coupling strength as in the interior.

With this reciprocal closing link, the cyclic spin Gauss generators are  $G_n^{\text{CBC}} = \tau_n^z - (s_{n,n+1}^z - s_{n-1,n}^z)$ , with cyclic link indices, and the accumulated field satisfies  $X_{L+1} = X_1$ . The CBC steady state in the fixed matter-number sector is

$$\rho_{\text{ss},N}^{\text{CBC}} = Z_{\text{CBC},N}^{-1} P_N \exp \left[ \sum_{n=1}^L X_n G_n^{\text{CBC}} \right] P_N. \quad (12)$$

Tracing out the links gives the same fixed- $N$  reduced matter distribution as Eq. (9). Hence the reduced matter steady occupation is unchanged:

$$N_{n,\text{CBC}}^{\text{ss}} = N_n^{\text{ss}}, \quad n = 1, \dots, L. \quad (13)$$

This equality is shown in Fig. 2(a), where the OBC and CBC steady occupations coincide.

The preservation of the reduced matter distribution does not hold in the nonzero Liouvillian spectrum: the full OBC and CBC spectra in Fig. 3 differ away from the zero mode. We now use the gauge-generated construction to compare the exact branch eigenoperators determined by the two boundary conditions and thereby identify the analytic signature for their nonzero spectral difference. Suppose that an operator-space transformation  $\mathcal{T}_\lambda[\rho] = T_\lambda \rho$  leaves  $\mathcal{L}_H$  invariant and satisfies  $(\mathcal{T}_\lambda \mathcal{L}_D \mathcal{T}_\lambda^{-1})[I] = \lambda I$ . Then  $\varrho_\lambda = \mathcal{T}_\lambda^{-1}[I]$  is a right eigenoperator of  $\mathcal{L}$  with eigenvalue  $\lambda$ . For the present link dissipator, each link has two local branches: the zero branch

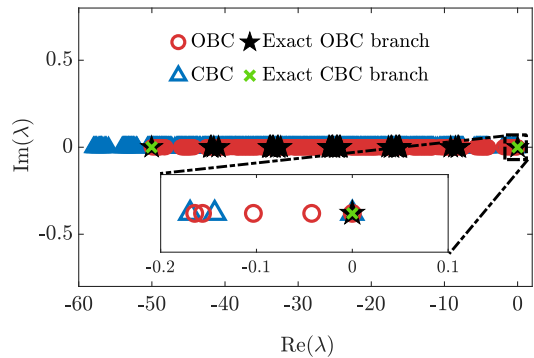


FIG. 3. Liouvillian spectra in the zero weak-gauge block at fixed matter number. Red: OBC. Blue: CBC. Black stars: exact OBC branch eigenvalues from Eq. (14). Green crosses: CBC branch eigenvalues obtained from the cycle-consistent branch assignments satisfying Eq. (15). The inset enlarges the zero-mode region. Parameters are the same as in Fig. 2(a).

$x_{0,n} = h_n$ ,  $\lambda_{0,n} = 0$ , and the nonzero branch  $x_{1,n} = i\pi$ ,  $\lambda_{1,n} = -2(\gamma_{u,n} + \gamma_{d,n})$ ; see Supplemental Material [47]. For OBC, the branch choice can be made independently on each interior link. Let  $k_n \in \{0, 1\}$ ,  $\mathbf{k} = k_1 k_2 \cdots k_{L-1}$ , and define  $X_1^{(\mathbf{k})} = 0$  and  $X_n^{(\mathbf{k})} = \sum_{m=1}^{n-1} x_{k_m, m}$  for  $n \geq 2$ . The corresponding exact OBC eigenoperator is

$$\varrho_{\mathbf{k}} = \exp \left[ \sum_{n=1}^L X_n^{(\mathbf{k})} G_n \right], \quad \lambda_{\mathbf{k}} = -2 \sum_{n=1}^{L-1} k_n (\gamma_{u,n} + \gamma_{d,n}). \quad (14)$$

The assignment  $\mathbf{k} = \mathbf{0}$  gives the steady state. Assignments with at least one  $k_n = 1$  give exact nonzero OBC eigenoperators, whose eigenvalues are marked by the black stars in Fig. 3. For a branch assignment under CBC, the factor  $\exp(\sum_{n=1}^L x_{k_n, n})$  must be single-valued after one loop. Equivalently,  $\sum_{n=1}^L x_{k_n, n}$  may change only by an integer multiple of  $2\pi i$ , which gives the cyclic consistency condition

$$\exp \left( \sum_{n=1}^L x_{k_n, n} \right) = 1. \quad (15)$$

For the zero branch, Eq. (15) reduces to  $\sum_{n=1}^L h_n = 0$ , which is precisely the accumulated-field consistency condition that determines the reciprocal CBC. For nonzero branch assignments under CBC, Eq. (15) imposes an additional cyclic consistency condition absent under OBC. The assignments satisfying this condition give the CBC branch eigenvalues marked by the green crosses in Fig. 3. The exact OBC branch eigenoperators associated with the black-star eigenvalues are generally not compatible with the same condition of Eq. (15) and have no CBC counterparts. The reciprocal CBC therefore preserves the reduced matter steady occupation through the zero branch, whereas the nonzero Liouvillian spectrum remains boundary-sensitive.

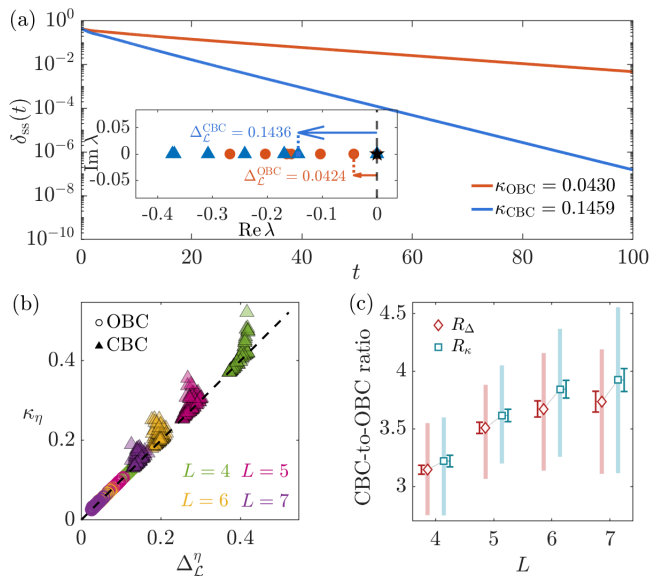


FIG. 4. Matter-occupation relaxation rates and Liouvillian gaps under OBC and reciprocal CBC. (a) Matter-occupation deviation  $\delta_{ss}^\eta(t)$  for one  $L = 7$  realization. The inset shows Liouvillian eigenvalues near  $\lambda = 0$ , with arrows marking  $\Delta_{\mathcal{L}}^{\text{OBC}}$  and  $\Delta_{\mathcal{L}}^{\text{CBC}}$ . (b) Late-time relaxation rates  $\kappa_\eta$  versus gaps  $\Delta_{\mathcal{L}}^\eta$ . Open circles denote OBC, filled triangles denote CBC, colors distinguish  $L = 4, 5, 6, 7$ , and the dashed line marks  $\kappa_\eta = \Delta_{\mathcal{L}}^\eta$ . (c) CBC-to-OBC ratios  $R_\Delta = \Delta_{\mathcal{L}}^{\text{CBC}}/\Delta_{\mathcal{L}}^{\text{OBC}}$  and  $R_\kappa = \kappa_{\text{CBC}}/\kappa_{\text{OBC}}$ . Markers, thick bars, and thin error bars denote means, interquartile ranges, and standard errors, respectively. All fitted dynamics start from the two leftmost matter sites occupied, all other matter sites empty, and all link spins in  $|\downarrow\rangle$ . Panels (b),(c) use 100 globally reciprocal Gaussian realizations with exact sample mean zero and sample variance  $\sigma_h^2 = 0.4$  for each  $L$ . Other parameters are  $J = 1$ ,  $\gamma = 2$ , and  $N = 2$ .

*Boundary-controlled relaxation.*— Within the fixed- $N$  zero weak-gauge block, relaxation toward the steady state is governed by the nonzero Liouvillian modes [13–15]. For  $\eta$  denotes OBC or CBC, let  $\rho_{ss,N}^\eta$  be the fixed- $N$  steady state and let  $R_j^\eta$  denote the nonzero right Liouvillian eigenoperators in the same block. Writing  $\rho^\eta(0) = \rho_{ss,N}^\eta + \sum_{j \geq 1} c_j^\eta R_j^\eta$  gives

$$\rho^\eta(t) = \rho_{ss,N}^\eta + \sum_{j \geq 1} c_j^\eta e^{\lambda_j^\eta t} R_j^\eta, \quad \mathcal{L}^\eta[R_j^\eta] = \lambda_j^\eta R_j^\eta. \quad (16)$$

Taking  $\text{Tr}(\hat{n}_n \cdot)$  and using Eq. (13) gives the deviation from the common steady occupation,  $N_n^\eta(t) - N_n^{\text{ss}} = \sum_{j \geq 1} c_j^\eta e^{\lambda_j^\eta t} \text{Tr}(\hat{n}_n R_j^\eta)$ . With Eq. (13), the above expansion converts the boundary-sensitive nonzero Liouvillian modes into boundary-controlled matter-occupation relaxation. We therefore quantify OBC and CBC relaxation by  $\delta_{ss}^\eta(t) = L^{-1} \sum_{n=1}^L |N_n^\eta(t) - N_n^{\text{ss}}|$ . Starting from the same initial matter occupations,  $\text{Tr}[\rho^\eta(0) \hat{n}_n] = N_n^{(0)}$ , we extract the fitted relaxation rate  $\kappa_\eta$  from the late-time tail  $\delta_{ss}^\eta(t) \sim A_\eta e^{-\kappa_\eta t}$  and compare it with the Li-

ouvillian gap  $\Delta_{\mathcal{L}}^\eta = \min_{\lambda_j^\eta \neq 0} [-\text{Re} \lambda_j^\eta]$ . For the initial states used below, the occupation dynamics contains a nonzero contribution from the slowest decaying mode, so the late-time relaxation rate follows the Liouvillian gap,  $\kappa_\eta \simeq \Delta_{\mathcal{L}}^\eta$  [13–15]. For one representative realization, Fig. 4(a) shows this gap-rate correspondence directly. In this realization,  $\delta_{ss}^\eta(t)$  decays for both boundary conditions toward the common steady occupation given by Eq. (13), and its late-time slopes agree with the smallest nonzero  $-\text{Re} \lambda$  in the inset of Fig. 4(a). The larger CBC gap therefore yields faster late-time relaxation of the matter-occupation profile in this realization.

We further verify that both the gap-rate correspondence and the faster CBC relaxation hold throughout the sampled globally reciprocal realizations. The fitted rates  $\kappa_\eta$  agree with the Liouvillian gaps  $\Delta_{\mathcal{L}}^\eta$  for both boundary conditions, as shown in Fig. 4(b). For the same interior realization, CBC gives both the larger gaps and fitted relaxation rates than OBC, and the sample-averaged CBC-to-OBC ratios remain above unity for  $L = 4, 5, 6, 7$ , as revealed in Fig. 4(b),(c). Thus the reciprocal closing link increases the late-time matter-occupation relaxation rate while leaving the reduced matter steady occupation unchanged.

In the strong-dissipation limit, the slow matter dynamics reduces to an effective fixed- $N$  exclusion process whose particle-transfer rates are set by the link pumping and loss [48–50], see Supplemental Material [47]. OBC contains transfers across the  $L - 1$  interior links, whereas the reciprocal CBC also includes the closing transfer between sites  $L$  and 1. For both boundary conditions, the fixed- $N$  matter-occupation steady distribution remains Eq. (9), since the reciprocal closing link leaves the matter-site values  $\{X_n\}$  unchanged. With this same steady distribution, the closing transfer adds a nonnegative term to the Dirichlet form [51], see Supplemental Material [47]. Hence the CBC exclusion process has a relaxation gap no smaller than OBC. This strong-dissipation result identifies the origin of the larger finite- $\gamma$  CBC gap,  $\Delta_{\mathcal{L}}^{\text{CBC}} > \Delta_{\mathcal{L}}^{\text{OBC}}$ , observed in the sampled realizations of Fig. 4. The boundary closure adds the closing transfer, while the accumulated field keeps the matter-occupation steady distribution fixed.

*Conclusions*— We have investigated a disordered dissipative quantum link chain with locally asymmetric but globally reciprocal link dissipation. The local dissipative asymmetries determine a realization-dependent accumulated field, which gives exact symmetry-resolved steady states and accumulated-field ordered reduced matter steady occupations through a gauge-generated transformation. The main result is that the same nonuniform reduced matter steady occupation can be reached under different boundary conditions, but with distinct relaxation rates toward it. The accumulated field fixes the reduced matter steady occupation, whereas the CBC changes the nonzero Liouvillian spectrum and thereby

the relaxation rate. In the strong-dissipation limit, this boundary-controlled relaxation is explained by a spectral comparison of effective exclusion processes with open and cyclic boundaries. The required matter-link dynamics and link-resolved pumping and loss are accessible in cold-atom and superconducting quantum-link platforms.

*Acknowledgments.*— This work was supported by the Joint Fund of Natural Science Foundation of Shandong Province (Grant No.ZR2024LLZ004), the National Natural Science Foundation of China(Grant No.12575010, No.12005110), and the Natural Science Foundation of Shandong Province (Grant No.ZR2020QA078, No.ZR2023MD064). The Youth Innovation Team Program of Shandong Province (Grant No.2023KJ118)

*Data Availability.*— The data that support the findings of this article are openly available [52], embargo periods may apply.

---

\* [zhaoxiaolong@qut.edu.cn](mailto:zhaoxiaolong@qut.edu.cn)

† [yixx@nenu.edu.cn](mailto:yixx@nenu.edu.cn)

- [1] E. J. Bergholtz, J. C. Budich, and F. K. Kunst, Exceptional topology of non-Hermitian systems, *Rev. Mod. Phys.* **93**, 015005 (2021).
- [2] N. Okuma and M. Sato, Non-Hermitian Topological Phenomena: A Review, *Annu. Rev. Condens. Matter Phys.* **14**, 83 (2023).
- [3] Y. Ashida, Z. Gong, and M. Ueda, Non-Hermitian physics, *Adv. Phys.* **69**, 249 (2020).
- [4] X. Zhang, T. Zhang, M.-H. Lu, and Y.-F. Chen, A review on non-Hermitian skin effect, *Adv. Phys.: X* **7**, 2109431 (2022).
- [5] S. Yao and Z. Wang, Edge states and topological invariants of non-Hermitian systems, *Phys. Rev. Lett.* **121**, 086803 (2018).
- [6] C. H. Lee and R. Thomale, Anatomy of skin modes and topology in non-Hermitian systems, *Phys. Rev. B* **99**, 201103(R) (2019).
- [7] F. K. Kunst, E. Edvardsson, J. C. Budich, and E. J. Bergholtz, Biorthogonal bulk-boundary correspondence in non-Hermitian systems, *Phys. Rev. Lett.* **121**, 026808 (2018).
- [8] F. Song, S. Yao, and Z. Wang, Non-Hermitian skin effect and chiral damping in open quantum systems, *Phys. Rev. Lett.* **123**, 170401 (2019).
- [9] A. Ghatak, M. Brandenbourger, J. van Wezel, and C. Coulais, Observation of non-Hermitian topology and its bulk-edge correspondence in an active mechanical metamaterial, *Proc. Natl. Acad. Sci. U.S.A.* **117**, 29561 (2020).
- [10] S. Weidemann, M. Kremer, T. Helbig, T. Hofmann, A. Stegmaier, R. Thomale, and A. Szameit, Topological funneling of light, *Science* **368**, 311 (2020).
- [11] L. Xiao, T. Deng, K. Wang, G. Zhu, Z. Wang, W. Yi, and P. Xue, Non-Hermitian bulk-boundary correspondence in quantum dynamics, *Nat. Phys.* **16**, 761 (2020).
- [12] T. Helbig, T. Hofmann, S. Imhof, M. Abdelghany, T. Kiessling, L. W. Molenkamp, C. H. Lee, A. Szameit, M. Greiter, and R. Thomale, Generalized bulk-boundary correspondence in non-Hermitian topoelectrical circuits, *Nat. Phys.* **16**, 747 (2020).
- [13] T. Haga, M. Nakagawa, R. Hamazaki, and M. Ueda, Liouvillian skin effect: Slowing down of relaxation processes without gap closing, *Phys. Rev. Lett.* **127**, 070402 (2021).
- [14] L. Mao, X. P. Yang, M.-J. Tao, H. P. Hu, and L. Pan, Liouvillian skin effect in a one-dimensional open many-body quantum system with generalized boundary conditions, *Phys. Rev. B* **110**, 045440 (2024).
- [15] X. Feng and S. Chen, Boundary-sensitive Lindbladians and relaxation dynamics, *Phys. Rev. B* **109**, 014313 (2024).
- [16] S. Longhi, Erratic Non-Hermitian Skin Localization, *Phys. Rev. Lett.* **134**, 196302 (2025).
- [17] S. Longhi, Erratic Liouvillian skin localization and subdiffusive transport, *Quantum Sci. Technol.* **11**, 025042 (2026).
- [18] Y. Z. Miao, W. Ding, L. T. Wang, X. L. Zhao, S. G. Liu, and X. X. Yi, Imaginary Gauge-steerable Edge Mode In Non-Hermitian Aubry-André-Harper Model, *Phys. Rev. A* **113**, 0535093 (2026).
- [19] W. N. Faugno and T. Ozawa, Interaction-induced non-Hermitian topological phases from a dynamical gauge field, *Phys. Rev. Lett.* **129**, 180401 (2022).
- [20] H. Li, H. Wu, W. Zheng, and W. Yi, Many-body non-Hermitian skin effect under dynamic gauge coupling, *Phys. Rev. Res.* **5**, 033173 (2023).
- [21] M. C. Zheng, Y. Qiao, Y. P. Wang, J. P. Cao, and S. Chen, Exact Solution of the Bose-Hubbard Model with Unidirectional Hopping, *Phys. Rev. Lett.* **132**, 086502 (2024).
- [22] H.-R. Wang, B. Li, F. Song, and Z. Wang, Scale-free non-Hermitian skin effect in a boundary-dissipated spin chain, *SciPost Phys.* **15**, 191 (2023).
- [23] J. B. Kogut, An introduction to lattice gauge theory and spin systems, *Rev. Mod. Phys.* **51**, 659 (1979).
- [24] J. B. Kogut, The lattice gauge theory approach to quantum chromodynamics, *Rev. Mod. Phys.* **55**, 775 (1983).
- [25] E. Fradkin, *Field Theories of Condensed Matter Physics* (Cambridge University Press, Cambridge, England, 2013).
- [26] D. Banerjee, M. Dalmonte, M. Müller, E. Rico, P. Stebler, U.-J. Wiese, and P. Zoller, Atomic Quantum Simulation of Dynamical Gauge Fields Coupled to Fermionic Matter: From String Breaking to Evolution after a Quench, *Phys. Rev. Lett.* **109**, 175302 (2012).
- [27] E. Zohar, J. I. Cirac, and B. Reznik, Quantum simulations of lattice gauge theories using ultracold atoms in optical lattices, *Rep. Prog. Phys.* **79**, 014401 (2015).
- [28] A. Mil, T. V. Zache, A. Hegde, A. Xia, R. P. Bhatt, M. K. Oberthaler, P. Hauke, J. Berges, and F. Jendrzejewski, A scalable realization of local U(1) gauge invariance in cold atomic mixtures, *Science* **367**, 1128 (2020).
- [29] B. Yang, H. Sun, R. Ott, H.-Y. Wang, T. V. Zache, J. C. Halimeh, Z.-S. Yuan, P. Hauke, and J.-W. Pan, Observation of gauge invariance in a 71-site Bose-Hubbard quantum simulator, *Nature* **587**, 392 (2020).
- [30] Z.-Y. Zhou, G.-X. Su, J. C. Halimeh, R. Ott, H. Sun, P. Hauke, B. Yang, Z.-S. Yuan, J. Berges, and J.-W. Pan, Thermalization dynamics of a gauge theory on a quantum simulator, *Science* **377**, 311 (2022).

- [31] P. Hauke, D. Marcos, M. Dalmonte, and P. Zoller, Quantum Simulation of a Lattice Schwinger Model in a Chain of Trapped Ions, *Phys. Rev. X* **3**, 041018 (2013).
- [32] E. A. Martinez, C. A. Muschik, P. Schindler, D. Nigg, A. Erhard, M. Heyl, P. Hauke, M. Dalmonte, T. Monz, P. Zoller *et al.*, Real-time dynamics of lattice gauge theories with a few-qubit quantum computer, *Nature* **534**, 516 (2016).
- [33] Y. T. Cheng and H. Zhai, Emergent  $U(1)$  lattice gauge theory in Rydberg atom arrays, *Nat. Rev. Phys.* **6**, 566 (2024).
- [34] D. Marcos, P. Rabl, E. Rico, and P. Zoller, Superconducting Circuits for Quantum Simulation of Dynamical Gauge Fields, *Phys. Rev. Lett.* **111**, 110504 (2013).
- [35] A. Blais, A. L. Grimsmo, S. M. Girvin, and A. Wallraff, Circuit quantum electrodynamics, *Rev. Mod. Phys.* **93**, 025005 (2021).
- [36] K. Stannigel, P. Hauke, D. Marcos, M. Hafezi, S. Diehl, M. Dalmonte, and P. Zoller, Constrained Dynamics via the Zeno Effect in Quantum Simulation: Implementing Non-Abelian Lattice Gauge Theories with Cold Atoms, *Phys. Rev. Lett.* **112**, 120406 (2014).
- [37] J. C. Halimeh and P. Hauke, Reliability of Lattice Gauge Theories, *Phys. Rev. Lett.* **125**, 030503 (2020).
- [38] J. C. Halimeh, R. Ott, I. P. McCulloch, B. Yang, and P. Hauke, Robustness of gauge-invariant dynamics against defects in ultracold-atom gauge theories, *Phys. Rev. Res.* **2**, 033361 (2020).
- [39] J. C. Halimeh, H. F. Lang, J. Mildenerger, Z. Jiang, and P. Hauke, Gauge-symmetry protection using single-body terms, *PRX Quantum* **2**, 040311 (2021).
- [40] N. Syassen, D. M. Bauer, M. Lettner, T. Volz, D. Dietze, J. J. García-Ripoll, J. I. Cirac, G. Rempe, and S. Dürr, Strong Dissipation Inhibits Losses and Induces Correlations in Cold Molecular Gases, *Science* **320**, 1329 (2008).
- [41] T. Tomita, S. Nakajima, Y. Takasu, and Y. Takahashi, Dissipative Bose-Hubbard system with intrinsic two-body loss, *Phys. Rev. A* **99**, 031601(R) (2019).
- [42] Z. J. Wang, X.-D. Dai, H.-R. Wang, and Z. Wang, Topologically ordered steady states in open quantum systems, *SciPost Phys.* **17**, 167 (2024).
- [43] X.-D. Dai, Z. J. Wang, H.-R. Wang, and Z. Wang, Steady-state topological order, *Phys. Rev. B* **111**, 115142 (2025).
- [44] Y.-M. Hu, Z. J. Wang, B. Lian, and Z. Wang, Many-Body Non-Hermitian Skin Effect with Exact Steady States in the Dissipative Quantum Link Model, *Phys. Rev. Lett.* **135**, 260401 (2025).
- [45] S. Chandrasekharan and U.-J. Wiese, Quantum link models: A discrete approach to gauge theories, *Nucl. Phys. B* **492**, 455 (1997).
- [46] Y. P. Huang, D. Banerjee, and M. Heyl, Dynamical Quantum Phase Transitions in  $U(1)$  Quantum Link Models, *Phys. Rev. Lett.* **122**, 250401 (2019).
- [47] See Supplemental Material for the derivation of the Liouvillian branch construction, the strong-dissipation effective exclusion process, and the OBC-to-CBC spectral comparison.
- [48] E. M. Kessler, Generalized Schrieffer-Wolff formalism for dissipative systems, *Phys. Rev. A* **86**, 012126 (2012).
- [49] G. M. Schütz, Exact solution of the master equation for the asymmetric exclusion process, *J. Stat. Phys.* **88**, 427 (1997).
- [50] B. Derrida, An exactly soluble non-equilibrium system: The asymmetric simple exclusion process, *Phys. Rep.* **301**, 65 (1998).
- [51] J. J. P. Veerman and R. Lyons, A Primer on Laplacian Dynamics in Directed Graphs, *Nonlinear Phenom. Complex Syst.* **23**, 196 (2020).
- [52] Y. Z. Miao and X. L. Zhao, Boundary-Controlled Liouvillian Relaxation with Exact Steady States Fixed by Dissipative Disorder data, [dataset], Zenodo (2026), [10.5281/zenodo.20779924](https://doi.org/10.5281/zenodo.20779924).